

SIMULATION OF COMPRESSIBLE FLOW USING A SEMI-IMPLICIT TVD SCHEME

E. Salimipour^{1*}, A. Salimipour²

¹ Department of Mechanical Engineering, Quchan University of Technology, Quchan, Iran

² Department of Mathematics, Quchan University of Technology, Quchan, Iran

ABSTRACT

Total variation diminishing (TVD) scheme is a kind of robust high-resolution approach, which removes the undesirable oscillations generated by numerical solution. The present work proposes a new implementation of the TVD scheme into a density-based semi-implicit finite-volume procedure to solve the inviscid and viscous flow equations. The proposed algorithm uses a simple linearization technique for convective fluxes. In order to enhance the accuracy of the algorithm, a high-resolution TVD scheme is employed in the discretization of the governing equations. This procedure has a simple implementation compared to other explicit and implicit schemes. The present scheme is first examined for some inviscid and viscous steady-state flows at several Mach numbers from subsonic to the supersonic regime. In addition, the inviscid and viscous unsteady flows are simulated and compared with experimental and numerical results, so that an acceptable correspondence was obtained. Results from this study indicate that the proposed algorithm is accurate for a wide range of Mach numbers.

KEYWORDS: *Density-based method; Semi-implicit; Finite-volume; Navier-Stokes equations; Total variation diminishing.*

1.0 INTRODUCTION

The flow equations typically solved in two general techniques of explicit and implicit in density-based methods. Implementations of the flow solution algorithm for implicit methods are commonly more difficult than the explicit ones, and for this reason, the flow simulations began with explicit procedures. Jameson was one of the earliest researchers who used explicit methods to solve the steady-state compressible inviscid flows (Jameson, 1981; 1983; 1991; Jameson & Yoon, 1986). He was commonly used dissipative terms for eliminating spurious oscillations, which were triggered by discontinuities in the solution. However, more stability and consequently, using the larger time steps in implicit methods cause to be attended by researchers. Another significant advantage of implicit schemes is their notable robustness and the rate of convergence in stiff equation systems or source terms, which are usually encountered in the simulations

*Corresponding author e-mail: esalimipour@qiet.ac.ir

of the real gases, turbulence modeling, or in highly stretched grids cases namely, high Reynolds number flows (Blazek, 2001).

Difficulties of the implicit methods are associated with the existence of nonlinear fluxes in the flow equations which need to be linearized. A popular method for linearization is the local Taylor expansion about the current time level. In one of the earliest works by Jespersen & Pulliam (1983), some linearizations for flux-vector splitting were analyzed using a numerical fixed-point iteration analysis. Their analysis showed that the use of approximate linearizations could be quite detrimental to stability and convergence of the numerical scheme. Yoon & Jameson (1986) developed a relaxation method using a multigrid method for the solution of the Euler equations. Their solution was based on a central difference scheme and did not need flux splitting.

The total variation diminishing (TVD) scheme is a high-resolution scheme, which acts very well on the unfavorable numerical errors in the solution of the flow equations, especially near the part where variables are discontinuous. Those numerical errors generally include numerical diffusion and oscillations when the numerical scheme is within the framework of the finite-volume method (Hou, Simons & Hinkelmann, 2012). Yee, Warming & Harten (1983) presented a detailed implementation of the implicit TVD scheme for the steady-state one- and two-dimensional compressible inviscid equations of gas dynamics. Their numerical results also indicated that the convergence rate is susceptible to the Courant–Friedrichs–Lewy (CFL) number. The iteration count had overgrown when the calculation was carried out away from an optimal time-step. A spatial discretization with third-order accuracy for the inviscid flux terms of the Euler equations used by Ravichandran (1997). He combined a Runge-Kutta time-stepping algorithm with the high-order spatial discretization to produce effective integration schemes for steady-state Euler computations. Teixeira & Alves (2012) carried out a procedure that generated steady-states with accurate far-field entrainment. An efficient and robust explicit time integration procedure for a high-order discontinuous Galerkin method was proposed by Renac et al. (2013) to solve the unsteady compressible Navier–Stokes equations. Kapen & Tchuen (2015) investigated an easy implementation method for the solution of the multi-dimensional Riemann problem for gas dynamics by use of the literal extension of the Toro Vazquez-Harten Lax Leer scheme.

A high-order TVD scheme is also a kind of robust high-resolution scheme, which removes the numerical errors by employing a limited flux to maintain monotonicity as well as high accuracy. The TVD concept introduced by Harten (1983) for ensuring monotonicity. This concept was then developed by Sweby (1984) using a flux limiter. This limiter consists of a limiter variable r and a limiter function Φ , which are presented as an r - Φ diagram. However, the TVD conditions are met only within a fixed part of this diagram. That means a group of schemes fulfill this law by laying the r - Φ into this TVD region, such as minmod, Van Leer, Van Albada, Superbee, and other schemes (Waterson & Deconinck, 2007). All of these schemes are derived based on the uniform grids. Hou et al. (2012) presented the TVD schemes for both uniform and unstructured grids. They also proposed an improved TVD scheme named WAHY. Zhang et al. (2015) proposed a refined r - factor algorithm for implementing the TVD schemes on arbitrary unstructured meshes based on the previous researches.

The above-mentioned studies were carried out for the steady-state solutions. Another disadvantage of explicit methods was appeared in solving unsteady problems, because of the lack of convergence in time steps. Jameson (2009) first implemented the dual-time

method for unsteady flows using an explicit multistage scheme accelerated by local time-stepping and multigrid. The significant advantage of this approach is that the physical time step is not restricted as usual in explicit methods. This method caused the convergence in each physical time step using an internal iteration loop. However, the dual-time stepping method increased CPU time.

Some of the existing implicit procedures have high speed to solve the steady-state flows due to using the large time steps. However, there are lots of unsteady problems, which do not need the large time steps and thus, implementation difficulties and use of huge computer memory are not affordable for these problems. This issue is especially crucial for solving three-dimensional problems or two-dimensional ones, which need the large computational grids. In this study, the implementation of a semi-implicit TVD scheme with a simple linearization technique is described in details. This procedure has some benefits as below:

- 1- Ease of implementation even against the existing explicit procedures
- 2- Use of high-resolution TVD schemes to prevent the numerical oscillations
- 3- Ease of coupling with other equations such as turbulence models, solid equations of motion (fluid-structure interaction) and two-phase flows.
- 4- No need to solve additional relations such as dissipative terms used in the central methods, Roe matrix, ...

To evaluate the present procedure, the Navier-Stokes equations are solved on a two-dimensional, unsteady, compressible flow by writing a computer code. Since an accurate validation is required for any numerical solver, several code validation studies are presented, including some cases of pressure and Mach number distributions and variations of lift, drag and pitching moment coefficients.

GOVERNING EQUATIONS

In this section, the numerical procedure used to compute the unsteady compressible flow is briefly described. The integral formulations for mass, momentum and energy conservation, in the non-dimensional form, are expressed as follows (Blazek, 2001):

$$\frac{\partial}{\partial \tau} \int_{\Omega} \vec{U} d\Omega + \oint_{\partial\Omega} (\vec{F}_c - \vec{F}_v) dS = 0 \quad (1)$$

where Ω is the control volume, bounded by the closed surface $\partial\Omega$, \vec{U} denotes the vector of the so-called conservative variables, and \vec{F}_c and \vec{F}_v are convection and viscous fluxes expressed as follows:

$$\vec{U} = \begin{bmatrix} \rho \\ \rho u \\ \rho v \\ \rho E \end{bmatrix}; \quad \vec{F}_c = \begin{bmatrix} \rho V \\ \rho u V + n_x p \\ \rho v V + n_y p \\ V(\rho E + p) \end{bmatrix}; \quad \vec{F}_v = \begin{bmatrix} 0 \\ n_x \tau_{xx} + n_y \tau_{xy} \\ n_x \tau_{yx} + n_y \tau_{yy} \\ n_x \theta_x + n_y \theta_y \end{bmatrix} \quad (2)$$

where V is defined as the scalar product of the velocity vector and the unit normal vector as follows:

$$V \equiv \vec{v} \cdot \vec{n} = n_x u + n_y v \quad (3)$$

with n_x and n_y being the components of the outward facing unit normal vector of the control surface $\partial\Omega$.

E is the total energy per unit mass and is defined as

$$E = \frac{p}{\rho(\gamma - 1)} + \left(\frac{u^2 + v^2}{2} \right) \quad (4)$$

The shear stress components, θ_x and θ_y are expressed as follows:

$$\tau_{xx} = 2\mu \frac{M_\infty}{\text{Re}} \left(\frac{\partial u}{\partial x} - \frac{\vec{\nabla} \cdot \vec{v}}{3} \right) \quad (5)$$

$$\tau_{yy} = 2\mu \frac{M_\infty}{\text{Re}} \left(\frac{\partial v}{\partial y} - \frac{\vec{\nabla} \cdot \vec{v}}{3} \right) \quad (6)$$

$$\tau_{xy} = \tau_{yx} = \mu \frac{M_\infty}{\text{Re}} \left(\frac{\partial u}{\partial y} + \frac{\partial v}{\partial x} \right) \quad (7)$$

$$\theta_x = u\tau_{xx} + v\tau_{xy} \quad (8)$$

$$\theta_y = u\tau_{yx} + v\tau_{yy} \quad (9)$$

All geometrical lengths are normalized with the size of characteristic length L , velocities with the free-stream speed of sound a_∞ , physical time (τ) with L/a_∞ , viscosity (μ) with μ_∞ , density (ρ) with ρ_∞ , and pressure (p) with $\rho_\infty a_\infty^2$.

IMPLICIT DISCRETIZATION OF THE GOVERNING EQUATIONS

The present semi-implicit algorithm is based on an iterative procedure. For simplicity, all the equations are developed in two-dimensional Cartesian coordinates. However, the algorithm and the underlying principle are general and can be applied to all structured (staggered or collocated) or unstructured grid systems. Performing spatial integration on the governing equation, over the control volume presented in Figure 1, leads to the following discrete equations:

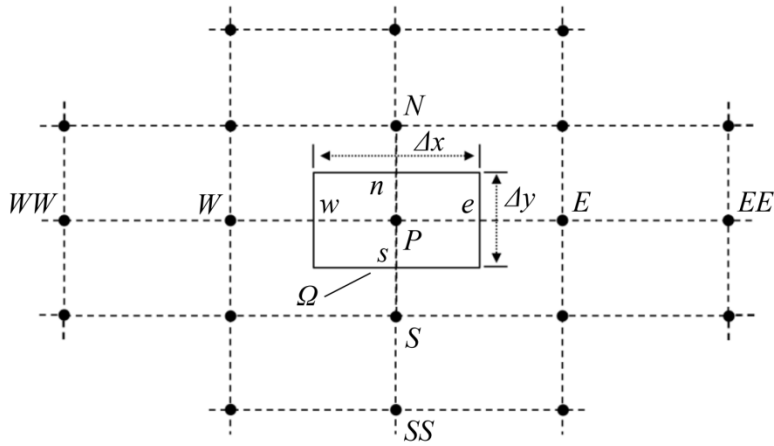


Figure 1. Control volume for the two-dimensional situation.

$$\frac{\vec{U}_P^{n+1} - \vec{U}_P^n}{\Delta t} \Delta x \Delta y + \vec{A}_e - \vec{A}_w + \vec{B}_n - \vec{B}_s = \vec{S} \quad (10)$$

where \vec{A} and \vec{B} are the nonlinear convective flux vectors and \vec{S} denotes the source term vector expressed as follows:

$$\vec{A} = \begin{bmatrix} \rho u \Delta y \\ \rho u u \Delta y \\ \rho u v \Delta y \\ \rho u E \Delta y \\ 0 \end{bmatrix}; \quad \vec{B} = \begin{bmatrix} \rho v \Delta x \\ \rho v u \Delta x \\ \rho v v \Delta x \\ \rho v E \Delta x \\ 0 \end{bmatrix}; \quad \vec{S} = \begin{bmatrix} [(\tau_{xx} - p)_e - (\tau_{xx} - p)_w] \Delta y + (\tau_{xy}_n - \tau_{xy}_s) \Delta x \\ (\tau_{yx}_e - \tau_{yx}_w) \Delta y + [(\tau_{yy} - p)_n - (\tau_{yy} - p)_s] \Delta x \\ [(\theta_x - up)_e - (\theta_x - up)_w] \Delta y + [(\theta_y - vp)_n - (\theta_y - vp)_s] \Delta x \end{bmatrix} \quad (11)$$

Equation (10) can be linearized as follow:

$$\frac{\vec{U}_P^{n+1} - \vec{U}_P^n}{\Delta t} \Delta x \Delta y + u_e^n \vec{U}_e^{n+1} \Delta y - u_w^n \vec{U}_w^{n+1} \Delta y + v_n^n \vec{U}_n^{n+1} \Delta x - v_s^n \vec{U}_s^{n+1} \Delta x = \vec{S}_P^n \quad (12)$$

with known faces velocities u_e , u_w , v_n and v_s from the previous iteration. subscripts e , w , n , s and p in Equation (12) are the locations as described in Figure 1.

To solve the linear equation (12), the conservative variables on the faces of the control volume, i.e., \vec{U}_e , \vec{U}_w , \vec{U}_n and \vec{U}_s must be approximated by the cell centers ones with high-order accuracy. There are various high-resolution limiter schemes such as essentially non-

oscillatory (ENO), weighted essentially non-oscillatory (WENO), normalized variable diagram (NVD) and total variation diminishing (TVD). The last case is one of the most robust schemes for capturing severe gradients in the flow-field.

3.1 Applying the TVD scheme

For uniform grids, the face value \vec{U}_e (between the cell centers P and E) is written in Roe's way (Roe, 1985). It consists of a diffusive first order upwind term and an anti-diffusive term:

$$\begin{aligned} \vec{U}_e &= \vec{U}_P + \frac{1}{2}\Phi(r_e)(\vec{U}_E - \vec{U}_P) ; u_e > 0 \\ \vec{U}_e &= \vec{U}_E + \frac{1}{2}\Phi(r_e)(\vec{U}_P - \vec{U}_E) ; u_e < 0 \end{aligned} \tag{13}$$

The upwind ratio r_e of consecutive differences of \vec{U} , can be expressed as follows:

$$\begin{aligned} r_e &= \frac{\vec{U}_P - \vec{U}_W}{\vec{U}_E - \vec{U}_P} ; u_e > 0 \\ r_e &= \frac{\vec{U}_E - \vec{U}_{EE}}{\vec{U}_P - \vec{U}_E} ; u_e < 0 \end{aligned} \tag{14}$$

Indeed, the anti-diffusive term in Equation (13) is a second-order correction term; however, the TVD conditions necessitate that the function Φ stays within the second-order TVD region and pass through the point (1,1) (Sweby, 1984) as shown in Figure 2. Some conventional TVD schemes are listed in below and also plotted in Figure 2.

Minmod (Harten, 1983)	$\Phi(r) = \max[0, \min(r, 1)]$
Superbee (Harten, 1983)	$\Phi(r) = \max[0, \min(2r, 1), \min(r, 2)]$
Van Leer (Waterson & Deconinck, 1983)	$\Phi(r) = (r + r)/(1 + r)$
Van Albada (Blazek, 2001)	$\Phi(r) = \max[0, (r + r^2)/(1 + r^2)]$

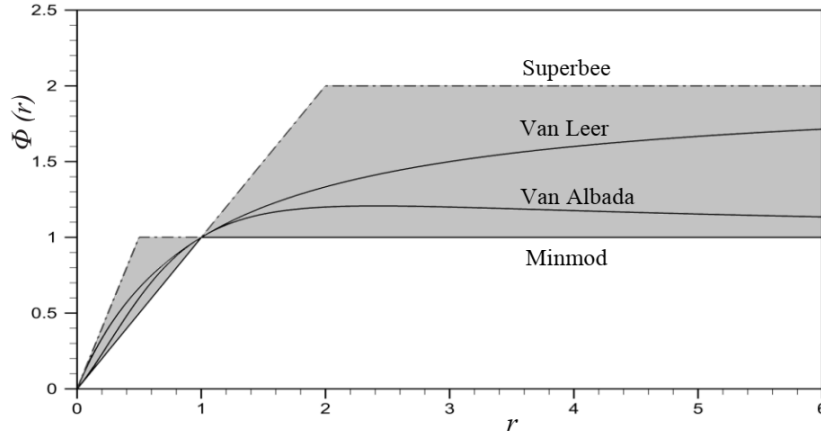


Figure 2. Second-order TVD region (grayed area) and some schemes.

3.2 Deriving linear equations system

With replacing the equation (13) into the equation (12) and considering the flow directions, the set of linear flow equations will be derived as follow:

$$a_P \vec{U}_P^{n+1} = a_E \vec{U}_E^{n+1} + a_W \vec{U}_W^{n+1} + a_N \vec{U}_N^{n+1} + a_S \vec{U}_S^{n+1} + \vec{b}^n \quad (15)$$

where

$$a_E = \max[0, -(1 - \phi(r_e)/2)u_e \Delta y] - \max[0, u_e \Delta y \phi(r_e)/2] \quad (16)$$

$$a_W = \max[0, (1 - \phi(r_w)/2)u_w \Delta y] - \max[0, -u_w \Delta y \phi(r_w)/2] \quad (17)$$

$$a_N = \max[0, -(1 - \phi(r_n)/2)v_n \Delta x] - \max[0, v_n \Delta x \phi(r_n)/2] \quad (18)$$

$$a_S = \max[0, (1 - \phi(r_s)/2)v_s \Delta x] - \max[0, -v_s \Delta x \phi(r_s)/2] \quad (19)$$

$$a_P = \Delta x \Delta y / \Delta t + a_E + a_W + a_N + a_S + (u_e - u_w) \Delta y + (v_n - v_s) \Delta x \quad (20)$$

$$\vec{b}^n = \vec{S}_P^n + \vec{U}_P^n \Delta x \Delta y / \Delta t \quad (21)$$

where a_E, a_w, \dots, a_{SS} and a_P are the 4×4 diagonal matrices for each grid cell. The set of equations (15) can be solved by various schemes such as Alternating Direction Implicit (ADI), Lower-Upper Symmetric Gauss-Seidel (LU-SGS), Generalized Minimal Residual (GMRES), etc. In this work, an ADI method is used. To dispose of the above procedure, an algorithm is presented for one time step as below:

- 1- Generate a computational grid,
- 2- Determine the distances of the grid cells (Δx and Δy),
- 3- Calculate the faces velocities (u_e, u_w, v_n and v_s),
- 4- Choose a TVD scheme ($\Phi(r)$),

- 5- Calculate the coefficients (relations (16-20)),
- 6- Calculate the source term (\vec{b}^n),
- 7- Form coefficient matrix (A),
- 8- Solve the set of equations $A\vec{U}^{n+1} = \vec{b}^n$,
- 9- Obtain the pressure from equation (4) and,

Iterate the steps (3-9) to reach convergence criteria.

RESULTS AND DISCUSSIONS

For the implementation of the numerical solution in the computational space, the present procedure is tested for some steady-state and unsteady flows. In all cases, the Van Albada TVD scheme was used. For steady-state and unsteady flows, the CFL number was set to 10 and 5, respectively.

4.1 Steady-state inviscid flows

The results of inviscid subsonic, transonic and supersonic flow calculations with the TVD scheme over a bump in a channel and on a NACA 0012 airfoil are presented. For the bump test, at the inlet of the channel, all flow variables are specified if a supersonic flow is considered. For subsonic inlet flow, stagnation pressure P_0 , stagnation temperature T_0 and the inlet angle are specified. At the outlet boundary, all the flow variables are extrapolated for the supersonic regime. The pressure is fixed for the subsonic outlet flows. Also, the slip boundary conditions are used on the upper and lower walls. A non-uniform grid of 90×30 in which the grid lines are closely packed in and near the bump region is shown in Figure 3.

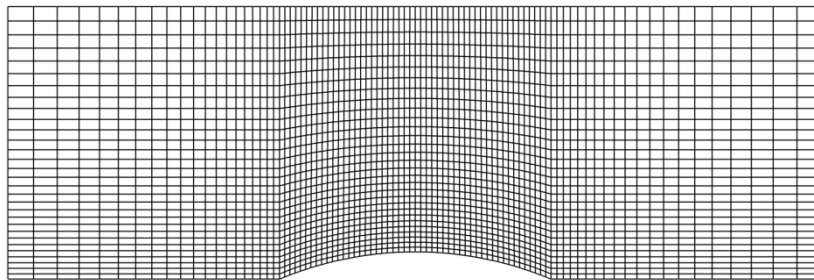


Figure 3. Bump geometry.

For the airfoil case, far-field boundary condition at the outlet and slip boundary conditions on the airfoil are used. A 340×40 C-type grid with excellent orthogonality is used in this case, so that the far-field boundaries were at least twenty chord lengths away. Figure 4 shows a close-up view of this grid.

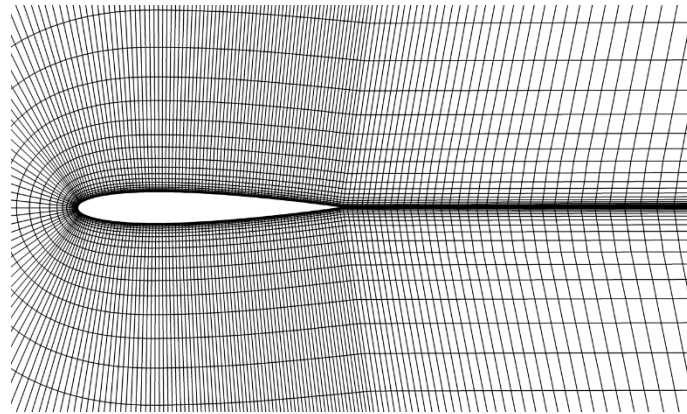


Figure 4. A view of C-type grid used in flow computations.

In the first test, static to stagnation pressure ratio was used to give a Mach number of 0.5 at the inlet of 10% thick bump. The Mach number distribution on the lower and upper walls are compared to TVD results obtained by Eidelman, Colella & Shreeve (1984) in Figure 5. It is seen that two Mach number distributions are very similar.

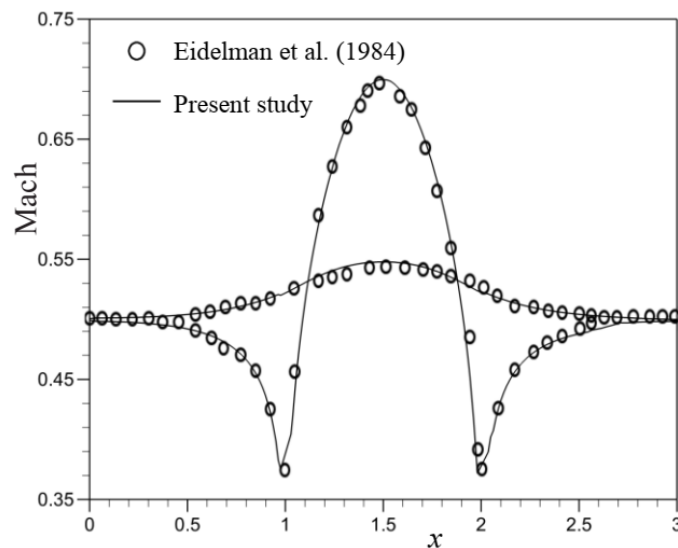


Figure 5. Mach number values on lower and upper walls of bump for $M_\infty=0.5$.

For the transonic test, flow past a NACA 0012 airfoil with free-stream Mach number of 0.8 and angle of attack $\alpha=1.25$ deg is solved and the pressure distribution is compared with TVD results by Pulliam & Steger (1985) in Figure 6. The results are very similar. Only the minimum pressure coefficient on the lower surface of the airfoil in the present study is 6% smaller. Locations of the shock waves can be seen on Mach contour distributions as shown in Figure 7.

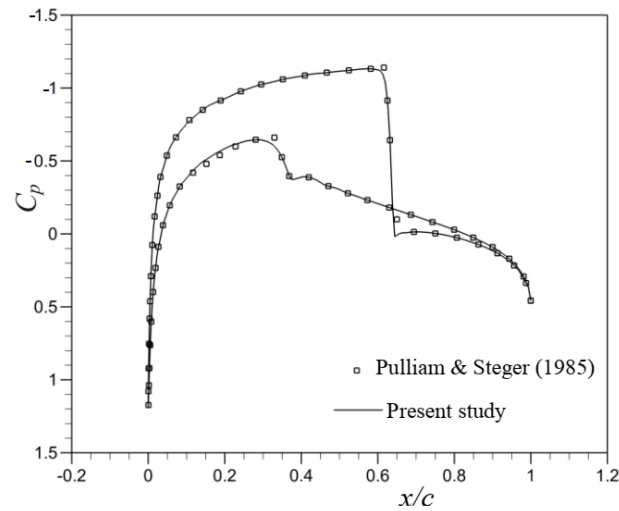


Figure 6. Pressure distribution on NACA 0012 airfoil for $M_\infty=0.8$ and $\alpha=1.25^\circ$.

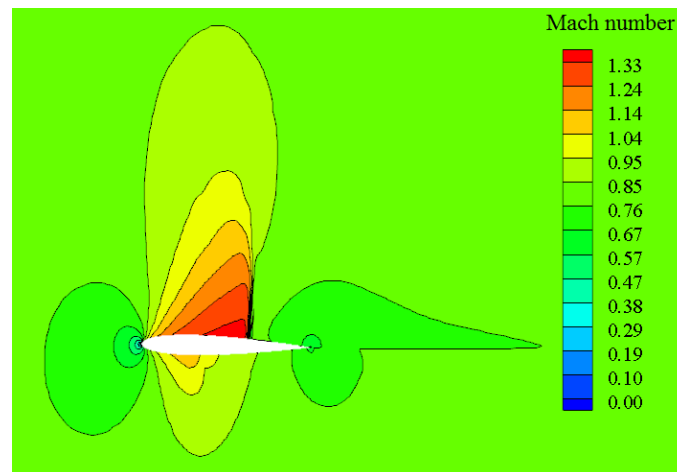


Figure 7. Contours of Mach number on NACA 0012 airfoil for $M_\infty=0.8$ and $\alpha=1.25^\circ$.

The third case is supersonic flow with $M_\infty=1.4$ over 4% thick bumps on a channel wall. Figure 8 shows the Mach number distribution on the upper and lower surfaces. These results are compared with the results of TVD scheme obtained by Djavarehshkian & Reza-zadeh (2007). This comparison shows that the resolution of the leading edge shock, the reflection of leading edge shock at the upper wall and trailing edge shock for two schemes are very close together. This verifies the validity of the present high-resolution scheme for supersonic flow.

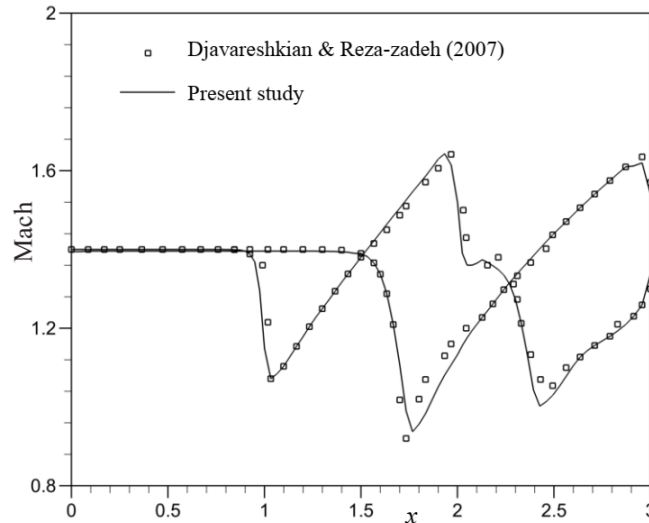


Figure 8. Mach number values on lower and upper walls of bump for $M_\infty=1.4$.

4.2 Steady-state viscous flows

The viscous flow calculations with the TVD scheme over a NACA 0008 airfoil and a circular cylinder are carried out at subsonic regime with $M_\infty=0.1$. No-slip conditions on the solid boundary are used. A 340×40 C-type grid and a 150×60 O-type grid are used in NACA 0008 airfoil and cylinder case, respectively. In the first viscous flow test, flow around a circular cylinder with $Re=40$ is simulated and the surface pressure distribution is compared to experimental data (Grove et al., 1964) and numerical results from (Sen, Mittal & Biswas, 2009) as shown in Figure 9.

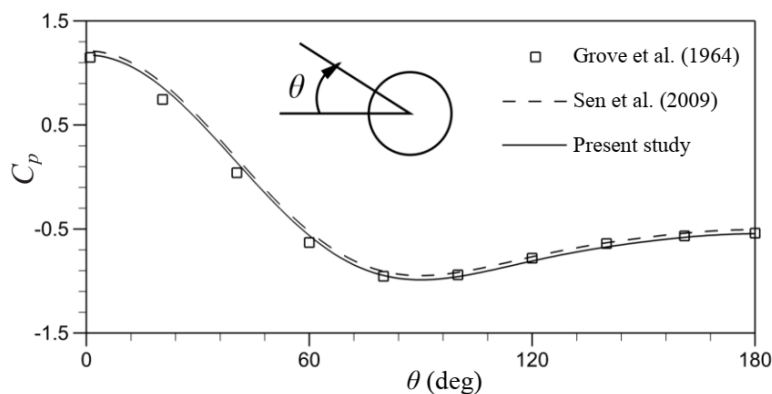


Figure 9. Pressure distribution on a circular cylinder for $Re=40$ and $M_\infty=0.1$.

The second viscous case is the flow past a NACA 0008 airfoil with chord-base $Re=6000$ and $\alpha=4$ deg. Figure 10 shows the temporal variation of the drag and lift coefficients. The simulations are run for a relatively large time duration of $\tau^*=\tau M_\infty=20$ at which point the force on the foil reaches a nearly constant value. These lift and drag coefficients are

compared with the numerical simulations by Mittal et al. (2008), and it is found that the current methodology provides a reasonably good prediction of these fundamental quantities.

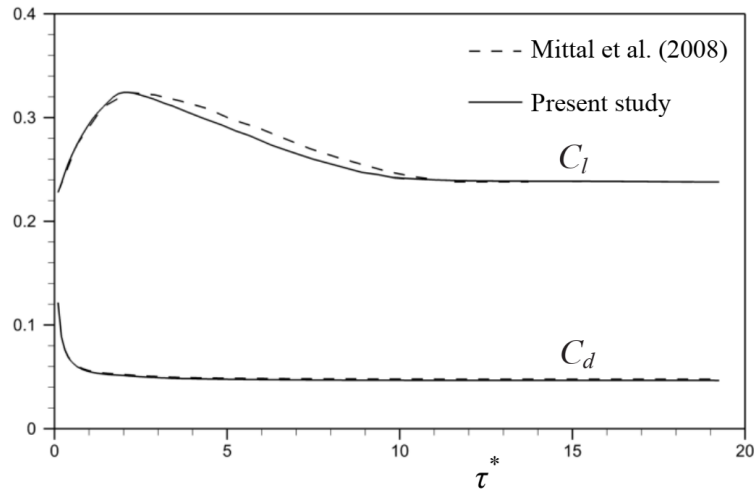


Figure 10. Temporal variation of drag and lift coefficients for NACA 0008 airfoil at $\alpha=4^\circ$ for $Re=6000$.

4.3 Unsteady inviscid flow

The present method is used to calculate the flow over a NACA 0012 airfoil pitching around its quarter-chord point. Experimental data were provided by Landon (1982). The following equation describes the pitching motion of the airfoil:

$$\alpha(t) = \alpha_m + \alpha_0 \sin(\omega t) \quad (22)$$

where α_m is the main angle of attack and α_0 is the angular amplitude. The angular frequency ω is related to the reduced frequency defined as follow:

$$k = \omega c / 2U_\infty \quad (23)$$

where c is the airfoil chord length. The grid used in the unsteady-flow calculations is the same as those used in the other steady-flow computations. The criterion for the convergence of the computations is that the maximum magnitude of the normalized residual must be reduced by more than six orders of magnitude as follow:

$$R(n) = \max \left(\left| \frac{\vec{U}_{k+1} - \vec{U}_k}{\vec{U}_{ref}} \right| \right) < 10^{-6} \quad (24)$$

where \vec{U}_{ref} is a reference value for \vec{U} and subscript k denotes the previous iteration. The present method is validated by comparing with numerical results obtained by Gao et al. (2005). Results are also compared with experimental data (Landon 1982). The airfoil is a

NACA 0012 pitching at the free-stream Mach number $M_\infty = 0.755$, $\alpha_m = 0.016$ deg, $\alpha_0 = 2.51$ deg, and $k = 0.0814$. The experimental $Re = 5.5 \times 10^6$. The comparisons of the present inviscid computations, numerical results (Gao et al., 2005) and the experimental data (Landon, 1982) of the instantaneous lift and moment coefficients versus the instantaneous angle of attack are presented in Figure 11. In order to observe the convergence process, the normalized residual is plotted in Figure 12. It can be seen that the convergence is well taken.

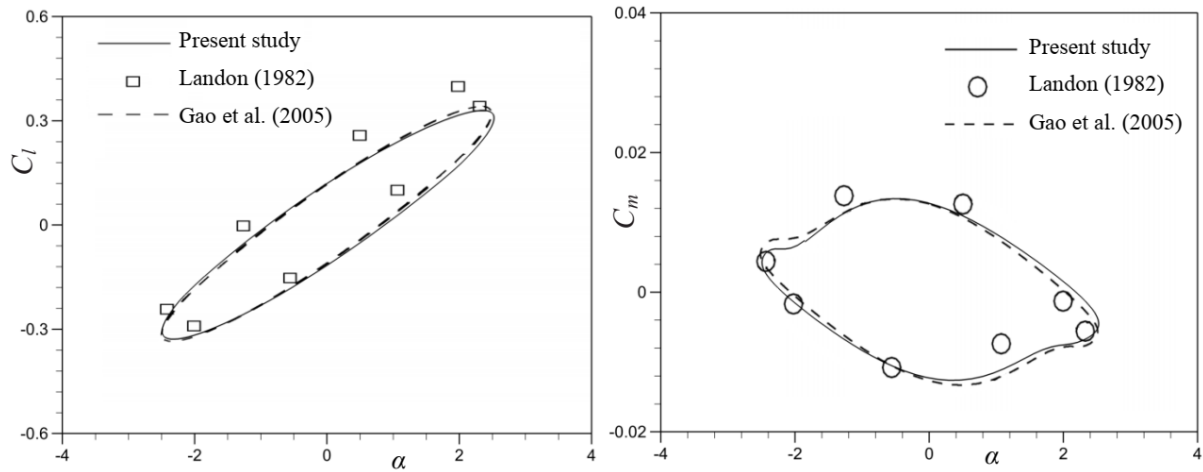


Figure 11. Comparison of lift and moment coefficients on NACA 0012 airfoil

$$M_\infty = 0.755, \alpha_m = 0.016 \text{ deg}, \alpha_0 = 2.51 \text{ deg}, k = 0.0814.$$

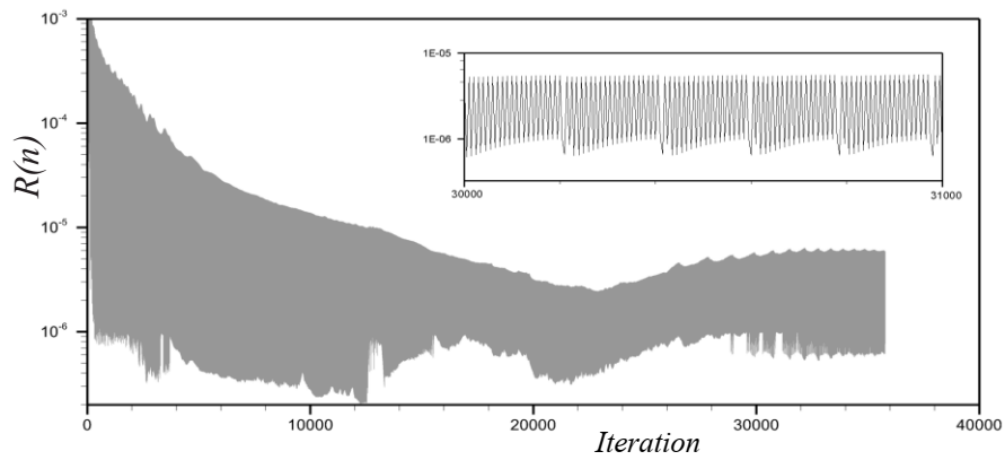


Figure 12. convergence process for NACA 0012 airfoil.

4.4 Unsteady viscous flow

In order to test the accuracy of the viscous flow solutions for the unsteady problem, a rotating circular cylinder is studied. Some calculations are carried out for $Re=200$ and ratio of the surface speed to free-stream velocity, $k = 0.5$ with an impulsive start. Streamlines for non-dimensional time $\tau^* = \tau M_\infty$ are compared with the experimental results from Coutanceau & Menard (1985) as shown in Figure 13. Good agreement is seen between the computational and experimental results for all times.

The next study is to compare the lift coefficients of a rotating cylinder with numerical results from (Teymourdash & Salimipour 2017). Since in this reference, an incompressible flow is simulated, a free-stream Mach number of 0.05 is used to prevent the compressibility effects. Figure 14 shows these comparisons with respect to the non-dimensional time τ^* for $0 \leq k \leq 5$ and $Re=200$. The results show excellent agreement.

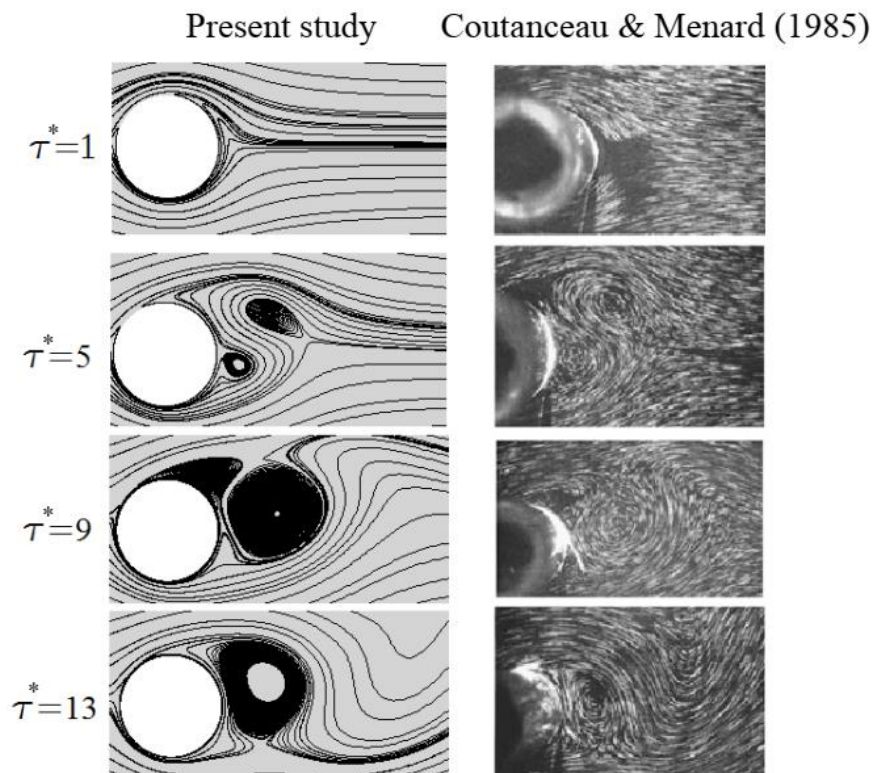


Figure 13. Comparison of instantaneous streamlines past a rotating cylinder for $\alpha=0.5$, $Re=200$ and $M_\infty=0.1$.

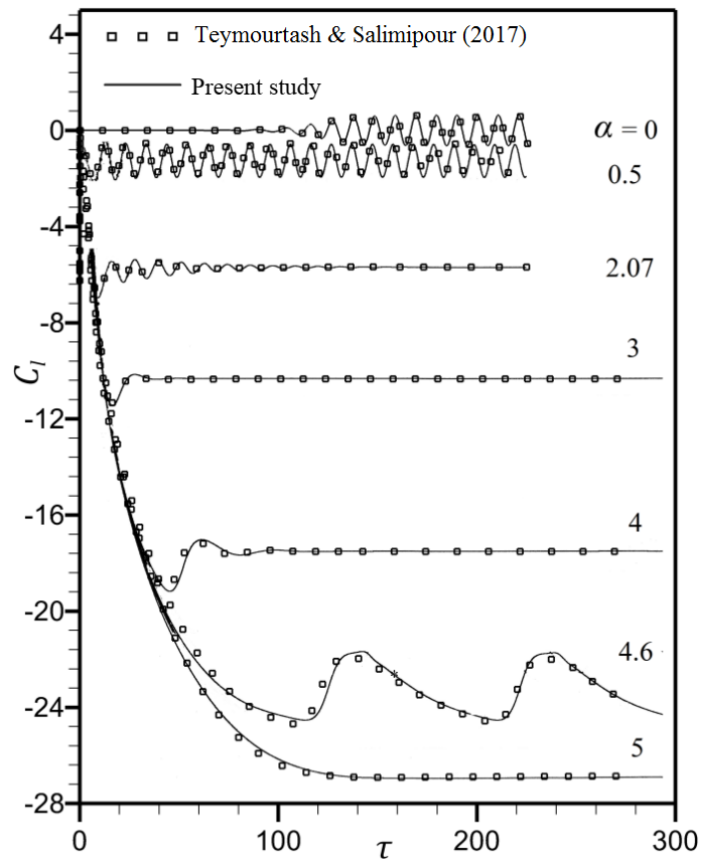


Figure 14. Comparison of cylinder lift coefficients for $k=0-5$ and $Re=200$.

CONCLUSIONS

A high-resolution scheme has been implemented in a density-based, finite-volume procedure which uses a semi-implicit solution algorithm. The mentioned scheme based on total variation diminishing (TVD) is developed to compute the fluxes of the convected quantities, including mass flux. The TVD scheme removes the undesirable oscillations generated by numerical errors, with preserving the solution accuracy. The method is applied to subsonic, transonic and supersonic flows, and the results have been compared with predicted data by the other TVD schemes based on the characteristic variable or experimental data. These comparisons show that the present high-resolution scheme predicts shock waves and unsteady boundary layer with high accuracy for both steady and unsteady flows. The discretization and the deriving linear equations system show that the present procedure can be easily implemented to solve the inviscid and viscous flows for a wide range of Mach numbers.

REFERENCES

- Blazek, J. (2001). *Computational Fluid Dynamics: Principles and Applications*. Amsterdam, London, New York: Elsevier.
- Coutanceau, M. & Menard, C. (1985). Influence of rotation on the near-wake development behind an impulsively started circular cylinder. *Journal of Fluid Mechanics*, 158, 399-466.
- Djavareshkian, M.H. & Reza-zadeh, S. (2007). Application of normalized flux in pressure-based algorithm. *Computers & Fluids*, 36, 1224–1234.
- Eidelman, S., Colella, P. & Shreeve, R.P. (1984). Application of the Godunov method and its second-order extension to cascade flow modeling. *AIAA journal*, 22(11), 1609–1615.
- Gao, C., Yang, S., Luo, S., Liu, F. & Schuster, D. (2005). Calculation of Airfoil Flutter by an Euler Method with Approximate Boundary Conditions. *AIAA journal*, 43(2), 295–305.
- Grove, A.S., Shair, F.H., Peterson, E.E. & Acrivos, A. (1964). An experimental investigation of the steady separated flow past a circular cylinder. *Journal of Fluid Mechanics*, 19, 60–80.
- Harten A. (1983). High resolution schemes for hyperbolic conservation laws. *Journal of Computational Physics*, 49, 357–393.
- Hou, J., Simons, F. & Hinkelmann, R. (2012). Improved total variation diminishing schemes for advection simulation on arbitrary grids. *International Journal for Numerical Methods in Fluids*, 70, 359–382.
- Jameson, A. & Yoon, S. (1986). LU implicit schemes with multiple grids for the Euler equations. *AIAA 24th aerospace sciences meeting*, 1-12.
- Jameson, A. (1981). Steady-state solution of the Euler equations for transonic flow. *Advances in scientific computing*, 37-70.
- Jameson, A. (1983). Numerical solution of the Euler equation for compressible inviscid fluids, *Princeton University, New Jersey 08544, USA*, 1-50.
- Jameson, A. (1991). Time-dependent calculations using multigrid, with applications to unsteady flows past airfoils and wings. *AIAA 10th computational fluid dynamics conference*, 1-12.
- Jameson, A. (2009). An Assessment of dual-time stepping, time spectral and artificial compressibility based numerical algorithms for unsteady flow with applications to flapping wings. *19th AIAA computational fluid dynamics conference*, 1-20.

- Jespersen, D.C. & Pulliam, T.H. (1983). Approximate Newton methods and flux vector splitting. *AIAA paper*, 83-1899.
- Kapen, P.T. & Tchien, G. (2015). An extension of the TV-HLL scheme for multi-dimensional compressible flows. *International Journal of Computational Fluid Dynamics*, 29(3-5), 303–312.
- Landon, R.H. (1982). NACA 0012 oscillating and transient pitching, compendium of unsteady aerodynamic measurements, Data Set 3. *AGARD*, Rept. R-702.
- Mittal, R., Dong, H., Bozkurtas, M., Najjar, F.M., Vargas, A. & Loebbecke, A. (2008). A versatile sharp interface immersed boundary method for incompressible flows with complex boundaries. *Journal of Computational Physics*, 227, 4825–4852.
- Pulliam, T.H. & Steger, J.L. (1985). Recent improvements in efficiency, accuracy, and convergence for implicit approximate factorization algorithms. *AIAA 23th aerospace sciences meeting*, 1-37.
- Ravichandran, K.S. (1997). Explicit Third Order Compact Upwind Difference Schemes for Compressible Flow Calculations. *International Journal of Computational Fluid Dynamics*, 8, 311–316.
- Renac, F., Gérald, S., Marmignon, C. & Coquel, F. (2013). Fast time implicit–explicit discontinuous Galerkin method for the compressible Navier–Stokes equations. *Journal of Computational Physics*, 251, 272–291.
- Roe P.L. (1985). Some contributions to the modeling of discontinuous flows. *Lectures in Applied Mathematics*, 22, 163–193.
- Sen, S., Mittal, S. & Biawas, G. (2009). Steady separated flow past a circular cylinder at low Reynolds numbers. *Journal of Fluid Mechanics*, 620, 89–119.
- Sweby P.K. (1984). High resolution schemes using flux limiters for hyperbolic conservation laws. *SIAM Journal on Numerical Analysis*, 21, 995–1011.
- Teixeira, R.S. & Alves, L.S.B. (2012). Modelling far-field entrainment in compressible flows. *International Journal of Computational Fluid Dynamics*, 26(1), 67–78.
- Teymourash, A.R. & Salimipour, S.E. (2017). Compressibility effects on the flow past a rotating cylinder. *Physics of Fluids*, 29, 016101.
- Waterson, N.P. & Deconinck, H. (2007). Design principles for bounded higher-order convection schemes – a unified approach. *Journal of Computational Physics*, 224, 182–207.

- Yee, H.C., Warming, R.F. & Harten, A. (1983). Implicit total variation diminishing (TVD) schemes for steady-state calculations. *NASA technical memorandum* 84342.
- Yoon, S. & Jameson, A. (1986). A multigrid LU-SSOR scheme for approximate Newton iteration applied to the Euler equations. *NASA-CR-179524*
- Zhang, Di., Jiang, Ch., Cheng, L. & Liang D. (2015). A refined r - factor algorithm for TVD schemes on arbitrary unstructured meshes. *International Journal for Numerical Methods in Fluids*, 80(2), 105-139.

NOMENCLATURE

a_∞	Free-stream speed of sound	u, v	Cartesian velocity components
c	Airfoil chord length	M_∞	Freestream Mach number
C_d	Drag coefficient	α	Angle of attack (deg)
C_l	Lift coefficient	θ	Surface angle respect to cylinder center
C_m	Moment coefficient	k	Ratio of surface speed to free-stream velocity
Re	Reynolds number	τ	Time
C_p	Pressure coefficient	—	Mean value superscript
p	Pressure		